Network: Computation in Neural Systems
March–June 2012; 23(1–2): 76–103

informa
healthcare

Analysis and Modelling of Multicellular Dynamics

Analysis and modelling of variability and covariability of population spike trains across multiple time scales

DMITRY R. LYAMZIN[1,2], JOSE A. GARCIA-LAZARO[1], & NICHOLAS A. LESICA[1]

[1]*Ear Institute, University College London, London, UK and* [2]*Division of Neurobiology, Department of Biology II, Ludwig-Maximilians-University Munich, Martinsried, Germany*

(Received 9 December 2011; revised 16 April 2012)

Abstract
As multi-electrode and imaging technology begin to provide us with simultaneous recordings of large neuronal populations, new methods for modelling such data must also be developed. We present a model of responses to repeated trials of a sensory stimulus based on thresholded Gaussian processes that allows for analysis and modelling of variability and covariability of population spike trains across multiple time scales. The model framework can be used to specify the values of many different variability measures including spike timing precision across trials, coefficient of variation of the interspike interval distribution, and Fano factor of spike counts for individual neurons, as well as signal and noise correlations and correlations of spike counts across multiple neurons. Using both simulated data and data from different stages of the mammalian auditory pathway, we demonstrate the range of possible independent manipulations of different variability measures, and explore how this range depends on the sensory stimulus. The model provides a powerful framework for the study of experimental and surrogate data and for analyzing dependencies between different statistical properties of neuronal populations.

Keywords: *Dichotomized Gaussian, noise correlations, population coding, Fano factor*

Correspondence: Nicholas A. Lesica, Ear Institute, University College London, 332 Gray's Inn Rd, London WC1X 8EE, UK. E-mail: n.lesica@ucl.ac.uk

ISSN 0954-898X print/ISSN 1361-6536 online/02/01-0200076–103 © 2012 Informa Healthcare Ltd.
DOI: 10.3109/0954898X.2012.679334

Introduction

In sensory systems repeated presentations of identical stimuli can evoke different spike patterns, with variability typically increasing from the periphery to more central brain areas (Kara et al. 2000). The importance of considering variability and covariability (or correlation) of spiking on different time scales has been stressed in a number of studies (Vaadia et al. 1995; Ratnam and Nelson 2000; Bair et al. 2001; Smith and Kohn 2008). For single neurons, the impact of variable spiking on stimulus coding has been studied on several time scales, from millisecond spike time jitter and phase-locking in early sensory pathways, to the scale of inter-spike intervals (ISIs) and spike counts across seconds in cortical areas (Softky and Koch 1993; Shadlen and Newsome 1998). Whether such variability is beneficial or detrimental for coding depends on the assumptions about the nature of the neural code and its significant parameters (Mainen and Sejnowski 1995; Schneidman et al. 1998; Manwani et al. 2002). When neuronal populations are considered, the same question arises with respect to the covariability of spiking of individual neurons (Zohary et al. 1994; Abbott and Dayan 1999; Romo et al. 2003; Schneidman et al. 2003; Latham and Nirenberg 2005; Averbeck et al. 2006). For populations of neurons, both spike synchrony on fine time scales and correlations in spike counts across longer time scales can result in synergistic or redundant coding depending, for example, on the similarity of the tuning curves of the neurons in the population (Zohary et al. 1994; Dan et al. 1998; Puchalla et al. 2005; Smith and Kohn 2008).

Taking this background into consideration, it is clear that tools enabling the analysis and modelling of the different types of variability in population spike trains should be developed. Previous research has shown that certain types of variability and covariability can be directly related to the spike train auto- and crosscorrelation functions (Bair et al. 2001; Nawrot 2010; Tchumatchenko et al. 2010). While existing models for the analysis of population spike trains allow specification of auto- and crosscorrelation functions (Krumin and Shoham 2009; Macke et al. 2009; Gutnisky and Josić 2010; Lyamzin et al. 2010) the parameters of these models have not yet been explicitly linked to the different measures of variability and covariability described above. Modelling spike trains with specified variability and covariability across multiple time scales, each of which could be independently manipulated, would provide a systematic way to study their impact on coding.

In this paper, we present further analysis of a model that we previously developed to capture instantaneous response properties of neuronal populations (Lyamzin et al. 2010). We show how the model can capture variability and covariability across a range of time scales, including signal to noise ratio, coefficient of variation (CV) of the ISI distribution, and Fano factor of spike counts for single neurons, and spike synchrony and correlation coefficient of spike counts for populations. Within the framework of our model, each of the variability and covariability measures can be expressed in terms of internal model parameters in closed form, and in particular, in terms of the auto- and crosscorrelation functions. Given experimental data, the model enables the simulation of spike trains with the same statistics, as well as manipulation of individual response properties. Furthermore, given a set of desired statistics, the model can be used to generate population spike trains *de novo*. Importantly, because the model is based on a dichotomized Gaussian framework, it enables not only simulation of spike trains, but also direct analysis of the relationship between different types of variability and covariability, and the impact of different

response properties on population coding. Matlab code implementing the model will be made available at www.ucl.ac.uk/ear/research/lesicalab.

Modelling experimental spike trains

Model framework

The basic framework of our model is described in our previous paper (Lyamzin et al. 2010). We represent spike trains as binary vectors of length N where each element corresponds to a time bin with a value of 1 if there is a spike and 0 otherwise. We assume the width of a time bin is small enough so that no more than one spike occurs in any time bin. Each stimulus is presented I times, so that for each cell a response to a single stimulus is a binary $N \times I$ matrix. We model a population of P cells, with binary vectors r_i^p for each cell p on each trial i obtained by thresholding a sum of Gaussian noise z_i^p that is different on each trial and a deterministic component s^p that is the same on each trial. Thresholding is done in each time bin $[n]$.

$$r_i^p[n] = \begin{cases} 1, & \left(s^p[n] + z_i^p[n]\right) > 0 \\ 0, & \left(s^p[n] + z_i^p[n]\right) \leq 0 \end{cases}$$

where $i = 1, \ldots, I$, $n = 1, \ldots, N$, and $p = 1, \ldots, P$. A schematic illustration of the model for single cells is shown in Figure 1.

The free parameters of this model are the values of s^p, which must be fit for each cell in each time bin, and the correlations in the Gaussian process z across both cells and time (the component of z corresponding to each cell is constrained to have unit variance across time).

The values of s^p are determined by the PSTH of each cell. From experimental data, one can calculate the PSTH ($\bar{r}^p$) and then find $s^p[n]$ by solving Equation (1) numerically in every time bin

$$\bar{r}^p[n] = \Phi(s^p[n], 1) \tag{1}$$

where $\Phi(x, \sigma^2)$ is the Gaussian cumulative distribution function with zero mean and variance σ^2 evaluated at x.

The correlations in z are determined by measuring the noise correlations in the spike trains. Correlations in the spike trains of sensory neurons have both signal and noise components, with signal correlations reflecting covariability in the stimulus-driven component of the response that is repeatable from trial to trial, and noise correlations reflecting covariability in the component of the response that is different from trial to trial. We assume that signal and noise correlations are additive, and thus define noise correlations between two spike trains as a difference between total correlations and signal correlations. Note that, although the dichotomized Gaussian framework can capture certain higher order statistical properties of spike trains (Macke et al. 2011, Yu et al. 2012), we assume for our purposes that only second order correlations are matched.

To set the correlations in the components of z corresponding to cells p and q at time lag k, $\rho_z^{pq}[k]$, one first measures the corresponding noise correlations from the

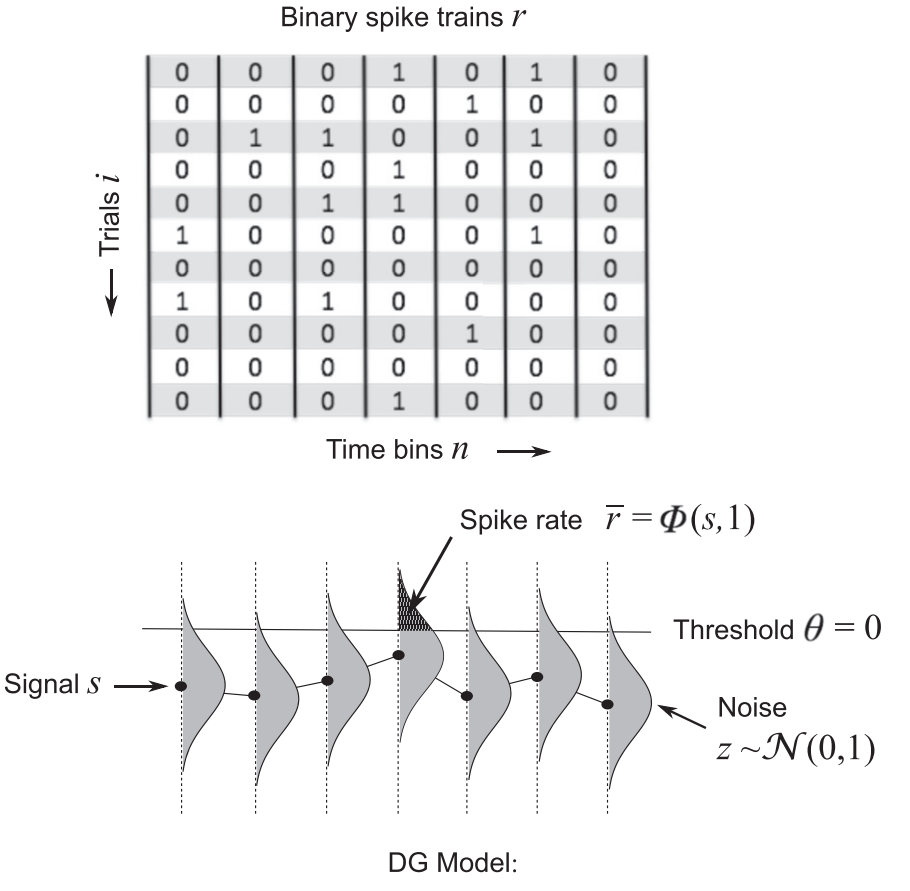

Figure 1. Schematic diagram of dichotomized Gaussian model for a single cell. The response of a cell to a single stimulus presentation is assumed to be represented by a binary vector r of length n, in which 1 corresponds to a time bin with a spike, and 0 corresponds to a time bin without a spike. The same stimulus is presented I times and the response of a cell on a particular trial in a particular time bin is denoted $r_i[n]$. Spikes are generated based on a Gaussian random 'noise' process z with unit variance, whose mean is different from time bin to time bin as specified by the value of a 'signal' s. In each time bin n, the probability of observing a spike across all trials (i.e. the PSTH) is given by the cumulative Gaussian distribution function evaluated at $s[n]$.

given set of spike trains:

$$\rho^{pq}_{noise}[k] = \rho^{pq}_{total}[k] - \rho^{pq}_{signal}[k]$$

which can be rewritten as

$$\rho^{pq}_{noise}[k] = \frac{\langle \mathrm{cov}(r_i^p, r_i^q(k)) \rangle_i}{\sqrt{\langle \mathrm{var}(r_i^p) \rangle_i \langle \mathrm{var}(r_i^q) \rangle_i}} - \frac{\langle \mathrm{cov}(r_i^p, r_i^q(k)) \rangle_{i \neq j}}{\sqrt{\langle \mathrm{var}(r_i^p) \rangle_i \langle \mathrm{var}(r_i^q) \rangle_i}} \quad (2)$$

where $\langle\cdot\rangle_i$ denotes the expected value of the covariance of two quantities on the same trial, $\langle\cdot\rangle_{i\neq j}$ denotes the expected value of the covariance of two quantities on different trials, and $r_i^p(k)$ is the vector r_i^p shifted by k time bins. Then one finds the corresponding $\rho_z^{pq}[k]$ by substituting (3) into (2) and solving numerically

$$\left\langle \mathrm{cov}\left(r_i^p, r_i^q(k)\right)\right\rangle_i = \left\langle \Phi_2\left(\begin{bmatrix} s^p[n] \\ s^q[n+k] \end{bmatrix}, \begin{bmatrix} 1 & \rho_z^{pq}[k] \\ \rho_z^{qp}[k] & 1 \end{bmatrix}\right)\right\rangle_n - r_0^p r_0^q \tag{3}$$

Variability of single cells on short time scales: Signal to noise ratio

In our previous paper, we specified the trial-to-trial variability of each cell as the signal to noise ratio

$$SNR = \frac{\mathrm{var}(\bar{r})}{\left\langle \mathrm{var}(\bar{r} - r_i)\right\rangle_i}$$

Because SNR is calculated for a single neuron, we omit cell indices for simplicity. We showed that, because the response is binary, if the PSTH is known, it uniquely defines SNR. This measure of variability is commonly used in the study of early sensory systems; it describes the reliability and precision of spiking across trials with respect to the stimulus. A cell with no noise, SNR $= \infty$, would spike on every trial in some bins, and never spike in the others. As the cell becomes less reliable, i.e. spikes are missed on some trials, or less precise, i.e. jitter moves spikes from one bin to the next, the SNR decreases. For a cell driven entirely by noise, i.e. a cell with a flat PSTH, the SNR is zero.

Variability of populations on short time scales: instantaneous signal and noise correlations

As described above, correlations in the spike trains of sensory neurons have both signal and noise components. In our previous paper, we specified the instantaneous signal and noise correlations, i.e. the correlations on the scale of a single time bin with zero lag $\rho_{signal}^{pq}[0]$ and $\rho_{noise}^{pq}[0]$. We showed that, because the responses are binary and the underlying noise process is Gaussian, matching the PSTH and signal to noise ratio of individual cells in the population will also match the instantaneous signal correlations between each pair. To match the instantaneous noise correlations between each pair of cells, the parameters $\rho_z^{pq}[0]$ that define the instantaneous correlations of z must be fit as described above.

Variability of single cells on long time scales: Fano Factor

The purpose of this paper is to analyze the relationship between the parameters of the Gaussian processes that underlie our model framework and experimentally relevant properties of spike trains that depend on temporal correlations – CV of the ISI distribution, Fano factor of spike counts, and correlation coefficient of spike counts for populations. For this purpose, one follows the fitting process described in the ''Model framework'' section to find the values of the covariance matrix of z not only with zero lag, but at all lags k that correspond to significant noise correlations.

To sample from the model and simulate spike trains, the correlated process z can be generated by using Gaussian conditioning (MacKay 2003; Macke et al. 2009; Lyamzin et al. 2010), or by using other methods, such as the multivariate autoregressive process described in (Gutnisky and Josić 2010).

Fano factor, the ratio of spike count variance to mean spike count across trials, has often been used as a measure of variability of spiking (Softky and Koch 1993; Berry et al. 1997; Shadlen and Newsome 1998; Kara et al. 2000). Fano factor is an obvious choice when neuronal activity is considered from the perspective of rate coding, and it has been used extensively to quantify variability in cortical cells, and, less commonly, cells of early sensory pathways. (Tolhurst et al. 1983; Sestokas and Lehmkuhle 1988; Hartveit and Heggelund 1994; Berry et al. 1997; Gur et al. 1997; Buracas et al. 1998; Gershon et al. 1998; Oram et al. 1999; Kara et al. 2000). A spike count distribution with a Fano factor equal to one has variability that is similar to that of a Poisson process, while neurons with Fano factors smaller than one are more reliable and those with high Fano factors are more variable.

Within the framework of our model, Fano factor can be expressed in terms of the correlation coefficients of z. Previous studies have shown that Fano factor depends on the integral of the spike train autocorrelation function, with Fano factor being bigger than one if the integral is positive, and less than one if the integral is negative (Macke et al. 2009). In our model, Fano factor depends not only on the integral of the autocorrelation function, but also, because the spike rate is not assumed to be stationary, on the value of s in every time bin.

The expression for Fano factor in terms of autocorrelations of the Gaussian process and signal can be written as (intermediate steps can be found in Appendix A):

$$FF = \frac{\sum_{n=1}^{N} \Phi(s[n],1) + 2\sum_{m=n+1}^{N}\sum_{n=1}^{N} \Phi_2\left(\begin{matrix}s[n]\\ s[m]\end{matrix}, \Sigma_z[m-n]\right) - \left(\sum_{n=1}^{N} \Phi(s[n],1)\right)^2}{\sum_{n=1}^{N} \Phi(s[n],1)} \tag{4}$$

Thus, given s in every time bin, when the autocorrelation function of a spike train is matched during the model fitting process, Fano factor is also matched. Modifying Fano factor will require changing the spike train correlation structure. Generally speaking, it can be changed arbitrarily, and in many cases simple scaling of correlation coefficients in $\Sigma_z[k]$ for all k is a valid method (note that not all Fano factors are realizable, as the covariance matrix of the underlying Gaussian process must remain valid; this limitation is discussed in detail in the ''Limitations of the model'' section). In the case of scaling, (4) can be converted into an equation in terms of the unknown scaling factor and solved numerically. The correlation matrix will then be parameterized by the scaling factor α,

$$\sum_{z}^{\alpha}[m-n] = \begin{bmatrix} 1 & \alpha\rho_z[m-n] \\ \alpha\rho_z[m-n] & 1 \end{bmatrix}$$

so that (4) can be rewritten as

$$FF(\alpha) = \frac{\sum_{n=1}^{N} \Phi(s[n],1) + 2\sum_{m=n+1}^{N}\sum_{n=1}^{N} \Phi_2\left(\begin{matrix}s[n]\\ s[m]\end{matrix}, \Sigma_z^{\alpha}[m-n]\right) - \left(\sum_{n=1}^{N} \Phi(s[n],1)\right)^2}{\sum_{n=1}^{N} \Phi(s[n],1)} \tag{5}$$

Thus, as long as the necessary scaling factor corresponds to a realizable autocorrelation function, one can create a new Gaussian random process that would produce spike trains with the desired Fano factor.

To demonstrate the ability of our model to both match and manipulate the Fano factor in experimental spike trains, we fit our model to responses from a single neuron in mouse auditory cortex. Spike trains were recorded during the presentation of a 100 repeated trials of a 1 second segment of an amplitude modulated broadband noise sound. Figure 2A shows a raster plot of the experimental responses.

Sampling spike trains (with the same trial length) from the fitted model resulted in responses with a Fano factor that matched the Fano factor in the original data, as shown in red in Figure 2B (dashed line is the line of equality, error bars denote two standard deviations of the values obtained by repeated bootstrap sampling). To demonstrate the ability of the model to manipulate the Fano factor in experimental data, we used Equation (5) to calculate a scaling factor for the autocorrelations of z such that the spike trains sampled from the model would have a different, predefined Fano factor. The responses of the model with scaled correlations accurately matched seven arbitrary values of Fano factor, including bigger and smaller values, as shown in black in Figure 2B.

Figure 2C shows histograms of spike counts for the two extreme cases of Fano factor modification shown in Figure 2B. The distribution of spike counts for $FF = 0.8$, the least variable example, is shown in blue bars. Spike counts are relatively tightly clustered around the mean count. The distribution of spike counts for the most variable example, $FF = 2.0$, is shown in white bars. The distribution is considerably wider and contains many more extreme values.

The effects of the change in Fano factor can be seen by eye in the corresponding raster plots. Figure 2D and E show the model responses with $FF = 0.8$ and $FF = 2.0$, respectively. The spike trains shown in Figure 2D are much more regular than those shown in Figure 2E, where one can see that a considerable proportion of spikes comes in bursts. Note that by design, instantaneous variability as measured by SNR is not affected by the manipulation of Fano factor: the SNR of the original data was 0.036, whereas the SNR of the manipulated data was 0.039 for $FF = 0.8$ and 0.032 for $FF = 2.0$. Similarly, the mean spike rate and PSTH are also unaffected.

Variability of single cells on short time scales: ISI distributions

Another important statistical property of the spike trains of individual cells is the distribution of ISIs. For the case of stationary spike rates, which is most commonly considered in the studies of ISI measures, ISI distributions are regularly shaped and are approximated well by gamma distributions (Nawrot et al. 2008; Shimokawa et al. 2010). The parameters of the gamma distribution in this case are defined by the autocorrelation function of the cell. Positive autocorrelations result in less regular spiking with ISI distributions that decrease monotonically with time. Negative autocorrelations result in more regular spiking, with the ISI distribution increasing with time for short ISIs, and then monotonically decreasing one once the peak has been passed.

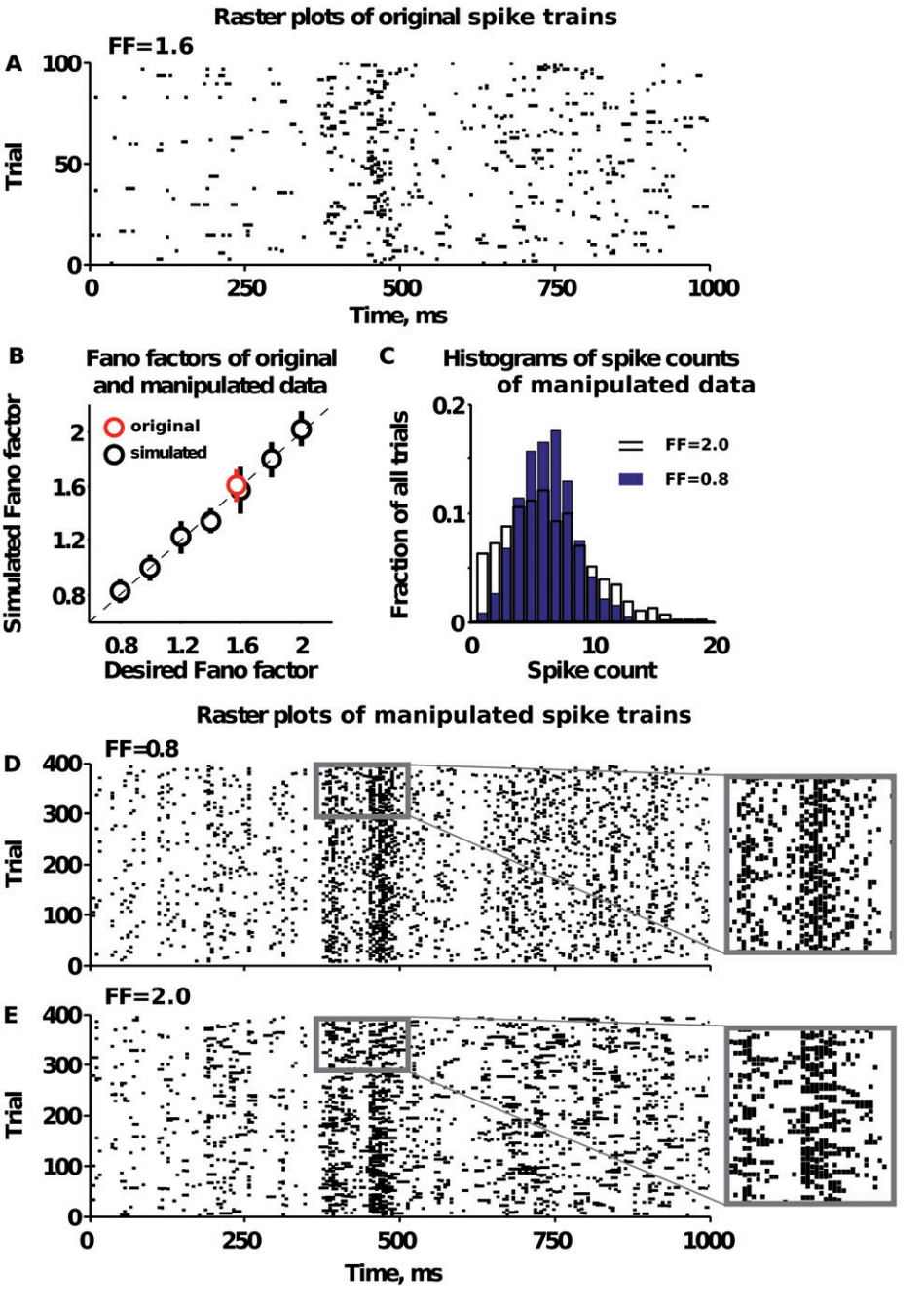

Figure 2. A. Raster plot of spike trains in mouse auditory cortex. The vertical axis specifies trial number, the horizontal axis specifies time since stimulus onset, and each dot on the plot represents a spike. The data were collected during the presentation of a 100 repeated trials of a 1 second segment of a sinusoidally modulated broadband noise sound. For model fitting, the data were binned in 5 ms time bins. B. Values of Fano factor from a simulated dataset versus desired value of Fano factor. We fitted our model to experimental data shown in Figure 2A, simulated spike trains with the same properties, and calculated Fano factor of the

continued

A useful landmark in the family of ISI distributions of cells with stationary spike rates is the distribution associated with Poisson spiking. In this case the distribution of ISIs is exponential with decay speed depending on the spike rate. In terms of coefficient of variation (CV), which is the ratio of standard deviation of a distribution to its mean, these spike trains, with CV equal to one, lie between positively autocorrelated, irregular, spike trains ($CV > 1$), and negatively correlated, regular, spike trains ($CV < 1$).

When spike rate is non-stationary, as is generally the case for sensory neurons, ISI distributions can be quite complex. An obvious example would be phase-locked spiking, where an ISI distribution can have several peaks at the ISIs that are multiples of the period of stimulus modulation. However, autocorrelations still have their own contribution in addition to the shape of the ISI distributions defined by the stimulus modulation. For example, as in the stationary spike rate case, negative autocorrelations due to refractoriness decrease the probability of short ISIs while increasing the probability of long ISIs, thus resulting in more regular spiking patterns (Berry et al. 1997).

For sensory systems, it is important to model spike trains with both refractoriness and flexible ISI variability in general. To characterize the regularity of spiking, we measure it with the squared coefficient of variation (CV^2) of the ISI distribution. Because of the generally non-stationary spike rate, CV^2 cannot be used to compare spiking regularity of different cells, but it is useful to measure the changes in spiking regularity of the same cell. The absolute value of CV^2 can also provide some guidelines on the statistics of a spike train, and choosing this measure is partially motivated by the ability to reference its values in limiting cases. For example, in addition to the Poisson case noted above, CV^2 is also a useful measure for comparing spike trains to renewal processes, for which CV^2 equals the Fano factor of spike counts.

In our model, we can derive explicit expressions for the probability of an ISI given s in every time bin and the autocorrelation function of the spike trains (assuming that the ISI distribution is completely determined by second order statistics). The probability of an ISI of length m time bins is the mean probability of this ISI length over all time bins n.

$$P(ISI = m) = \left\langle P(ISI[n] = m) \right\rangle_n$$

figure continued
original and simulated data. The corresponding point is plotted in red. We set 7 other arbitrary values (from 0.8 to 2.0), solved for the scaling factor of each, simulated spike trains for every autocorrelation found, and plotted the Fano factor calculated from the simulated spike trains versus the desired Fano factor (in black). C. Spread of spike counts for the simulated datasets with $FF = 0.8$ and $FF = 2.0$. Blue bars show the distribution of spike counts for the simulated data with $FF = 0.8$, transparent bars with black edges show the distribution of spike counts for the simulated data with $FF = 2.0$. D. Raster plot of the simulated dataset where the autocorrelation function was scaled to match Fano factor value of 0.8. A magnified part of this raster plot is shown to the right. E. Raster plot of the simulated dataset where autocorrelation function was scaled to match Fano factor value of 2.0, presented as in D.

These probabilities are calculated as follows:

$$\begin{aligned} P(ISI = m) &= \left\langle P(ISI[n] = m) \right\rangle_n \\ P(ISI[n] = m) &= P(r[n+1, n+2, \ldots, n+m] = [0, \ldots, 1] | r[n] = 1) \\ &= \frac{1}{P(r[n] = 1)} P(r[n, n+1, \ldots, n+m] = [10, \ldots, 01]) \\ &= \frac{1}{\bar{r}[n]} \int_{-\infty}^{s[n]} \underbrace{\int_{s[n+1]}^{+\infty} \ldots}_{m-1} \int_{-\infty}^{s[n+m]} \mathcal{N}(0, \Sigma) \mathrm{d}x \end{aligned}$$

where

$$\Sigma = \begin{bmatrix} 1 & \rho_z[1] & \cdots & \rho_z[m] \\ \rho_z[1] & 1 & & \rho_z[m-1] \\ \vdots & & \ddots & \\ \rho_z[m] & \rho_z[m-1] & & 1 \end{bmatrix} \tag{6}$$

Thus, the probability distribution of ISIs, and hence its coefficient of variation, is matched as long as the autocorrelation function of the spike trains is matched, to the extent that the ISI distribution depends only on the second order statistics of the intrinsic noise.

Modifying the CV^2 of an ISI distribution is done by manipulating the correlation coefficients of z. As in the case of Fano factor, this can be done by arbitrary changes of correlation structure, but often works with scaling: all correlation coefficients in the covariance matrix of z are multiplied by a parameter.

$$\Sigma^{\alpha} = \begin{bmatrix} 1 & \alpha\rho_z[1] & \cdots & \alpha\rho_z[m] \\ \alpha\rho_z[1] & 1 & & \alpha\rho_z[m-1] \\ \vdots & & \ddots & \\ \alpha\rho_z[m] & \alpha\rho_z[m-1] & & 1 \end{bmatrix}$$

and the probability of an ISI of length m at a given time bin n with a spike is

$$P(\alpha) = P(ISI[n] = m) = \frac{1}{\bar{r}[n]} \int_{-\infty}^{s[n]} \underbrace{\int_{s[n+1]}^{+\infty} \ldots}_{m-1} \int_{-\infty}^{s[n+m]} \mathcal{N}(0, \Sigma^{\alpha}) \mathrm{d}x$$

Once the desired value of CV^2 is specified, the value of the scaling factor can be found numerically from the following formula.

$$CV^2(\alpha) = \frac{\mathrm{var}(P(\alpha))}{\left\langle P(\alpha) \right\rangle^2} \tag{7}$$

Where $P(\alpha)$ is the probability distribution of ISIs as a function of the scaling parameter α.

Obviously, for independent manipulation of CV^2 and FF, modification of the correlations of z via simple scaling is not suitable. In this case, one has to use modifications of the correlations of z that have two free parameters. One such example is discussed in the "Independent manipulation of CV^2 and FF" section.

To demonstrate the ability of our model to match and manipulate the ISI distribution of experimental data, we fit our model to a set of spike trains from a single cell in mouse inferior colliculus (IC). Spike trains were recorded during the presentation of 100 repeated trials of a 1 second segment of amplitude modulated broadband noise sounds (see raster in Figure 3A).

With the assumption of the ISI distribution being defined by second order statistics, we match the signal component and autocorrelation function and thus the ISI distribution. The ISI distribution of the original data and the data sampled from the fitted model are shown in Figure 3B. The original distribution of ISIs is shown in blue bars, and the distribution of ISIs sampled from the fitted model is shown by the black and white line. The CV^2 of the original data is 0.40 and CV^2 of the data sampled from the fitted model is 0.38.

Figure 3C demonstrates how scaling of the autocorrelations can change the CV^2 of the spike trains. We found the scaling factor of the autocorrelation function that would produce spike trains with CV^2 of 0.3 and 1.0, thus increasing and decreasing spiking regularity respectively. The resulting distributions of ISIs are compared with the original in Figure 3C. (Note that depending on the length of a trial in time bins, the use of sampling in the numerical search for the parameter value in the Equation (7) can be computationally more efficient than calculation of the ISI probability distribution by using the Equations (6). The results shown in Figure 3C were obtained by sampling the spike trains with scaled correlation coefficients and calculating the ISI probability distribution directly from these spike trains.)

The effects of changes in the CV^2 of the ISI distribution can be seen on the raster plots in Figure 3D and E. In the case of CV^2 of 1.0, there is no observed refractoriness and spiking often occurs in bursts due to strong positive autocorrelations, as can be seen in the inset in Figure 3D. For $CV^2 = 0.3$, spiking becomes more refractory, as can be seen in the inset in Figure 3E; almost every spike has a period of silence of one or more time bins, which is the result of increased negative noise autocorrelations.

Variability of populations on long time scales: Count correlations

The effects of noise correlations on population coding can be studied across multiple time scales (Bair et al. 2001; Averbeck et al. 2006; Smith and Kohn 2008). In our previous work (Lyamzin et al. 2010), we mainly addressed instantaneous correlations that are related to spiking synchrony between two cells. One can also consider correlations that are calculated from larger time bins or whole trials. Correlations in spike counts across seconds have the capacity to both increase and decrease the information carried by a population depending on the correlation structure across the population, and the perspective from which their effect is studied (Abbott and Dayan 1999).

As with the variability measures for individual cells described above, the pairwise count correlations for a population of cells can be related to the covariance matrix of the noise process z.

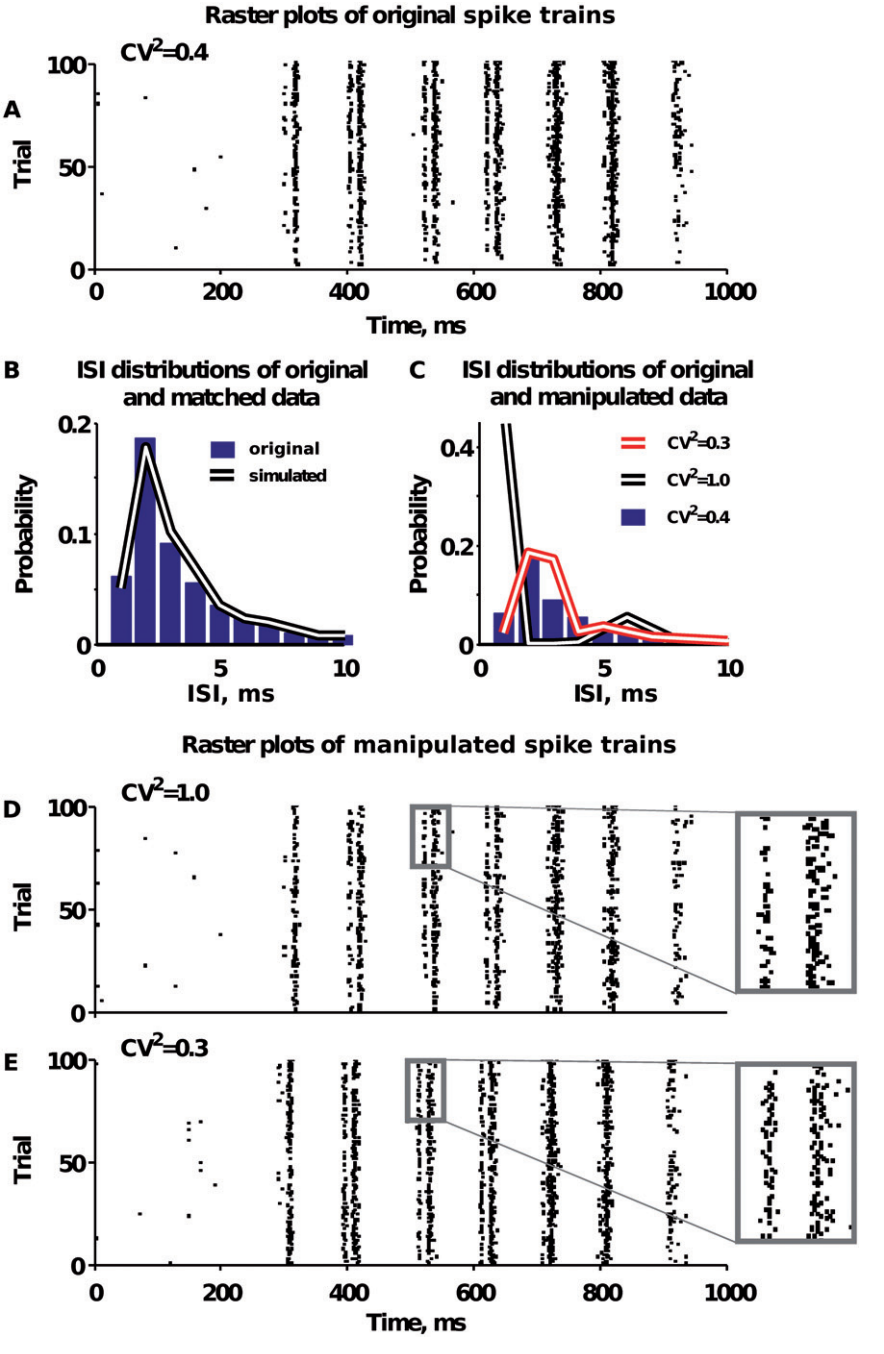

Figure 3. A. Raster plot of spike trains in mouse inferior colliculus. The data were collected during the presentation of a 100 repeated trials of a 1 second segment of a sinusoidally modulated broadband noise sound. For model fitting, the data were binned in 1 ms time bins. B. ISI distribution of original data (blue bars), and ISI distribution of spike trains sampled from the model fitted to the original data (black and white line). C. ISI distribution of original data (blue bars), and ISI distribution of manipulated data (black and white, red and white lines). Given the parameters of the fitted model, we solved for the scaling coefficient of autocorrelation function that would give us the desired value of CV^2 of the ISI distribution: 0.3 and 1.0, with CV^2 calculated for the same range of time bins where the autocorrelations are significant ($k = 10$). D. Raster plot of the simulated dataset where autocorrelation function was scaled to match CV^2 value of 1.0. E. Raster plot of the simulated dataset where autocorrelation function was scaled to match CV^2 value of 0.3.

Count correlations are defined as

$$CC = \frac{\mathrm{cov}\left(\sum_{n=1}^{N} r^p[n],\ \sum_{m=1}^{N} r^q[m]\right)}{\sqrt{\mathrm{var}\left(\sum_{n=1}^{N} r^p[n]\right)\mathrm{var}\left(\sum_{m=1}^{N} r^q[m]\right)}} = \frac{\left\langle\left(\sum_{n=1}^{N} r^p[n]\right)\left(\sum_{m=1}^{N} r^q[m]\right)\right\rangle - \left\langle\sum_{n=1}^{N} r^p[n]\right\rangle\left\langle\sum_{m=1}^{N} r^q[m]\right\rangle}{\sqrt{\mathrm{var}\left(\sum_{n=1}^{N} r^p[n]\right)\mathrm{var}\left(\sum_{m=1}^{N} r^q[m]\right)}}$$

First, we expand the product of spike counts:

$$\left\langle\sum_{n=1}^{N} r^p[n]\sum_{m=1}^{N} r^q[m]\right\rangle = \left\langle r^p[1]r^q[1] + r^p[1]r^q[2] + \cdots + r^p[n]r^q[m] + \cdots + r^p[N]r^q[N]\right\rangle$$

and express each of the $r^p[n]r^q[m]$ products in terms of cumulative distributions:

$$\left\langle\sum_{n=1}^{N} r^p[n]\right\rangle = \sum_{n=1}^{N}\Phi(s^p[n], 1)$$

$$\left\langle\sum_{n=1}^{N} r^p[n]\sum_{m=1}^{N} r^q[m]\right\rangle = \sum_{m=1}^{N}\sum_{n=1}^{N}\Phi_2\left(\begin{matrix}s^p[n]\\ s^q[m]\end{matrix}, \Sigma_z[m-n]\right)$$

The formula for count correlations can then be rewritten as

$$CC = \frac{\sum_{m=1}^{N}\sum_{n=1}^{N}\Phi_2\left(\begin{matrix}s^p[n]\\ s^q[m]\end{matrix}, \Sigma_z[m-n]\right) - \sum_{n=1}^{N}\Phi(s^p[n], 1)\sum_{m=1}^{N}\Phi(s^q[m], 1)}{\sqrt{\mathrm{var}\left(\sum_{n=1}^{N} r^p[n]\right)\mathrm{var}\left(\sum_{m=1}^{N} r^q[m]\right)}} \quad (8)$$

where assuming symmetry of correlations

$$\Sigma_z[m-n] = \begin{bmatrix} 1 & \rho_z^{pq}[m-n] \\ \rho_z^{qp}[m-n] & 1 \end{bmatrix}$$

and

$$\mathrm{var}\left(\sum_{n=1}^{N} r^p[n]\right) = \sum_{n=1}^{N}\Phi(s^p[n], 1) + \sum_{n=1}^{N}\sum_{m=1}^{N}\Phi_2\left(\begin{matrix}s^p[n]\\ s^q[m]\end{matrix}, \Sigma_z[m-n]\right) - \left(\sum_{n=1}^{N}\Phi(s^p[n], 1)\right)^2$$

Count correlations depend only on s and the crosscorrelation function between two cells. Thus, when the crosscorrelation function between two neurons is matched during the model fitting process, the count correlations are also matched.

As in the case of the single cell properties described above, manipulation of count correlations can often be achieved by finding a scaling factor for the

crosscorrelations of z that will result in spike trains with the desired count correlations. The covariance matrix in this case is rewritten as

$$\Sigma_z^{\alpha}[m-n] = \begin{bmatrix} 1 & \alpha\rho_z^{pq}[m-n] \\ \alpha\rho_z^{qp}[m-n] & 1 \end{bmatrix}$$

where α is the scaling factor, and the variance of spike counts can be rewritten as

$$\mathrm{var}\left(\sum_{n=1}^{N} r^p[n]\right) = \sum_{n=1}^{N} \Phi(s^p[n],1) + \sum_{n=1}^{N}\sum_{m=1}^{N} \Phi_2\left(\begin{matrix} s^p[n] \\ s^q[m] \end{matrix}, \Sigma_z^{\alpha}[m-n]\right) - \left(\sum_{n=1}^{N} \Phi(s^p[n],1)\right)^2$$

so that the count correlation value from (8) now depends on the scaling factor

$$CC(\alpha) = \frac{\sum_{m=1}^{N}\sum_{n=1}^{N} \Phi_2\left(\begin{matrix} s^p[n] \\ s^q[m] \end{matrix}, \Sigma_z^{\alpha}[m-n]\right) - \sum_{n=1}^{N} \Phi(s^p[n],1) \sum_{m=1}^{N} \Phi(s^p[m],1)}{\sqrt{\mathrm{var}\left(\sum_{n=1}^{N} r^p[n]\right)\mathrm{var}\left(\sum_{m=1}^{N} r^q[m]\right)}} \tag{9}$$

Equation (9) can be solved for α numerically.

When the scaling factor of the crosscorrelation function is found, one can create a new Gaussian random process z that would produce spike trains with the required value of count correlations.

To demonstrate the ability of our model to both match and manipulate pairwise count correlations in experimental spike trains, we fit our model to responses from a pair of neurons in gerbil auditory cortex. Spike trains were recorded during the presentation of a 100 repeated trials of a 200 ms segment of an amplitude modulated broadband noise sound (see raster plots in Figure 4A).

Sampling spike trains (with the same trial length) from the fitted model resulted in responses with a count correlation coefficient that matched the count correlation coefficient in the original data, as shown in red in Figure 4B. We also used Equation (9) to calculate the scaling factor for the autocorrelations of z such that the result of sampling from the model would have a different, predefined count correlation coefficient. The responses of the model with scaled correlations accurately matched four arbitrary values of correlation coefficient, including bigger and smaller values, as shown in black in Figure 4B.

The difference between the two extreme simulated cases (count correlation of 0.4 and 0.7) can be seen from the plot of the joint spike count distributions in Figure 4C and D (colored contours represent levels of equal probability, points within red contours correspond to the most frequently occurring pairs of spike count values, and points within blue contours correspond to less frequently occurring pairs of spike count values). The distribution of spike counts for spike trains with $CC = 0.7$ shown in Figure 4C is more elongated along the diagonal than the distribution for spike trains with $CC = 0.4$ shown in Figure 4D.

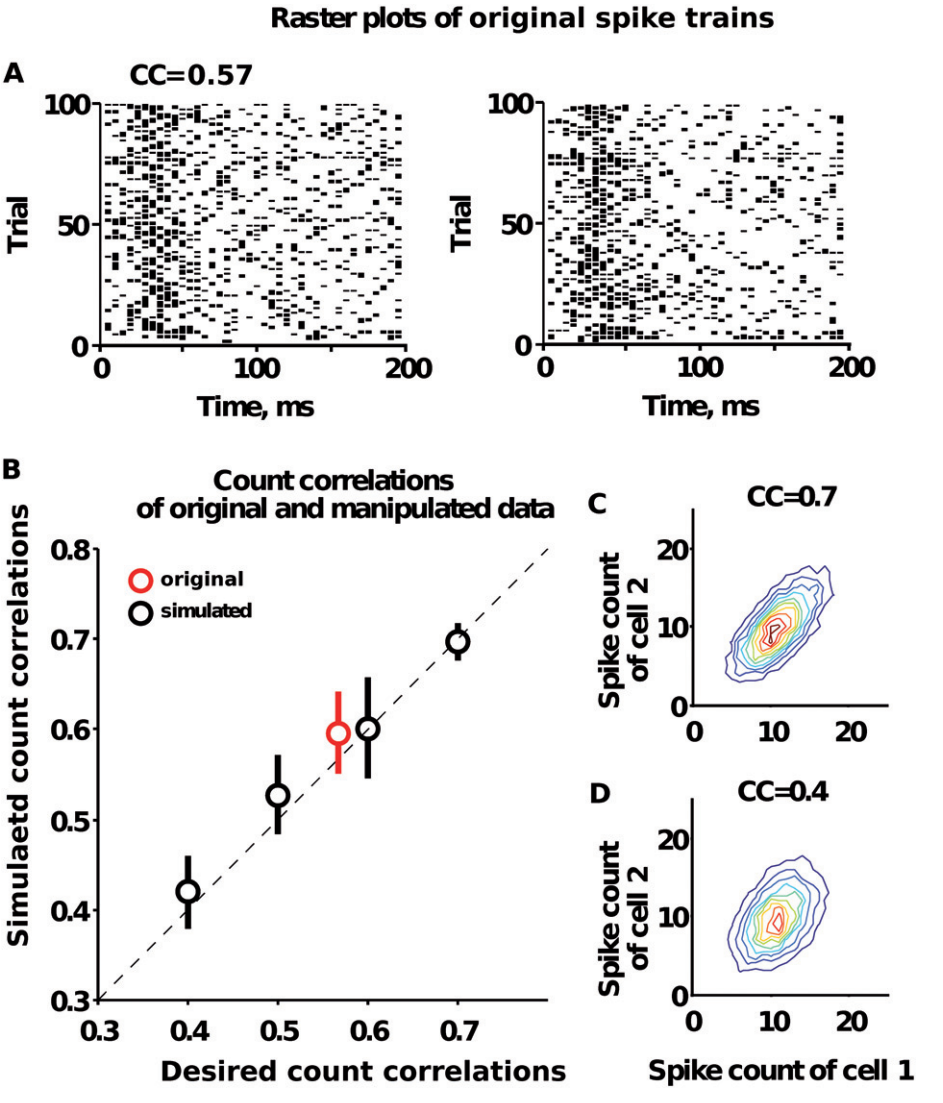

Figure 4. A Raster plot of the spike trains from a pair of cells in gerbil auditory cortex. The data were collected during the presentation of 100 repeated trials of a 200 second segment of a sinusoidally modulated broadband noise sound. The data were binned in 5 ms time bins. B. Matching the desired values of count correlations. The horizontal axis shows the desired value of count correlation coefficient and vertical axis shows the count correlation coefficient of the simulated spike trains. We fitted our model to the original data and sampled spike trains from the fitted model. The count correlation of the simulated spike trains is plotted versus the count correlation coefficient of the original spike train in red. We set four other arbitrary values from 0.4 to 0.7 and solved for the scaling coefficient of the autocorrelation function that would yield the desired count correlation in the simulated spike trains. The count correlations calculated from the simulated spike trains are plotted versus the desired values of correlations in black. Dashed line is the line of equality C, D. Contour plots of the distributions of spike counts of two cells. For the count correlations of 0.7 (C) and 0.4 (D) we created two-dimensional histograms of the spike counts of both cells with the spike count of cell one on the horizontal axis, and the spike count of cell 2 on the vertical axis. C and D show these histograms as contour plots, where each line denotes a level of constant probability of falling inside the contour.

Simulating spike trains *de novo*

Model framework

In addition to matching and manipulating a particular set of experimental data, the model can also be used to generate a new spike trains with a desired set of statistics. Unlike the data-based model in which the PSTH of each neuron and several associated quantities are constrained to match those observed experimentally, the *de novo* version of the model provides a fully flexible framework in which to investigate the interaction of variability and covariability on different time scales.

In recent studies (De La Rocha et al. 2007) it has been shown, both theoretically and experimentally, that correlations between two cells depend on their spike rates. Within our the dichotomized Gaussian framework, this dependency also holds (Macke et al. 2011). The advantage of our model is that similar relationships can be observed for a wider range of parameters, e.g. SNR, signal correlations, Fano factors etc. Additionally, our model can also be used to study how values of a given parameter constrain the possible range of the others.

The model used for simulation of spike trains *de novo* is a modification of the one described above. A version of this model with specified instantaneous variability and covariability was described in detail in our previous work (Lyamzin et al. 2010). As before, spike trains are generated as binary matrices by thresholding a sum of a signal s that is the same on every trial and a noise z that is different on every trial.

$$r_i^p[n] = \begin{cases} 1, & \left(s^p[n] + z_i^p[n]\right) > \theta^p \\ 0, & \left(s^p[n] + z_i^p[n]\right) \leq \theta^p \end{cases}$$

where $i = 1, \ldots, I$, $n = 1, \ldots, N$, and $p = 1, \ldots, P$.

The PSTH of each cell is no longer constrained by the experimental responses, but must be defined in another way. One can simply choose an arbitrary deterministic signal to create a pseudo-experimental situation, or choose a parametric stochastic signal to allow precise control of the relevant spike train parameters. For the latter case, we set s to be a Gaussian process with variance $\sigma_{s^p}^2$ that is a free parameter for each cell. In this case, as both the mean spike rate r_0 and the SNR are no longer constrained by the PSTH, a second free parameter is required in the form of a variable threshold θ^p. Both *SNR* and r_0 can be expressed in terms of $\sigma_{s^p}^2$ and θ^p (Lyamzin et al. 2010) and the required values solved for numerically.

Because instantaneous signal correlations are also no longer defined by the PSTHs of the two cells, ρ_{signal}^{pq} becomes a free parameter of the spike trains, which can be manipulated by changing the corresponding ρ_s^{pq}, the correlation coefficient between the different components of s. In the previous paper, we showed that for Gaussian s, ρ_{signal}^{pq} and ρ_{noise}^{pq} can be expressed in terms of ρ_s^{pq} and ρ_z^{pq}. Hence, given the desired values of ρ_{signal}^{pq} and ρ_{noise}^{pq}, one can generate the correlated s and z processes that would give spike trains with desired correlations after thresholding.

Fano factor of de novo spike trains

If we assume the signal s is Gaussian, we can write closed form expressions for the same measures of variability and covariability presented in the ''Modelling

experimental spike trains'' section. Fano factor can be written out as

$$FF = \frac{\sum_{n=1}^{N} \Phi(-\theta, \sigma_s^2 + 1) + \sum_{n \neq m}^{N} \Phi_2\left(\begin{matrix}-\theta \\ -\theta\end{matrix}, \Sigma_{s+z}[m-n]\right) - \left(\sum_{n=1}^{N} \Phi(-\theta, \sigma_s^2 + 1)\right)^2}{\left(\sum_{n=1}^{N} \Phi(-\theta, \sigma_s^2 + 1)\right)}$$

The correlation matrix of the two-dimensional Gaussian now contains correlation coefficients of s and z, as well as the variance of s. For derivation and details, see Appendix B. Using this formula for cases when s can be assumed to be Gaussian can dramatically decrease calculation times.

ISI distribution of de novo spike trains

In the case of *de novo* generation of spike trains with Gaussian s, we can write out the probability of finding an ISI of a certain length m analogous to the ''Fano factor of *de novo* spike trains'' section (again assuming that the ISI distribution is determined only by second order statistics)

$$P(ISI = m) = \left\langle P(ISI[n] = m) \right\rangle_n$$

where

$$\begin{aligned} P(ISI = m) &= \left\langle P(ISI[n] = m) \right\rangle_n \\ P(ISI[n] = m) &= P(r[n+1, n+2, \ldots, n+m] = [0, \ldots, 1] | r[n] = 1) \\ &= \frac{1}{P(r[n] = 1)} P(r[n, n+1, \ldots, n+m] = [10, \ldots, 01]) \\ &= \frac{1}{r_0} \int_{-\infty}^{-\theta} \underbrace{\int_{-\theta}^{+\infty} \ldots}_{m-1} \int_{-\infty}^{-\theta} \mathcal{N}(0, \Sigma_{s+z}) \mathrm{d}x \end{aligned}$$

and

$$\Sigma_{s+z} = \begin{bmatrix} 1 + \sigma_s^2 & \rho_z[1] + \sigma_s^2 \rho_s[1] & \cdots & \rho_z[k] + \sigma_s^2 \rho_s[k] \\ \rho_z[1] + \sigma_s^2 \rho_s[1] & 1 + \sigma_s^2 & & \rho_z[k-1] + \sigma_s^2 \rho_s[k-1] \\ \vdots & & \ddots & \\ \rho_z[k] + \sigma_s^2 \rho_s[k] & \rho_z[k-1] + \sigma_s^2 \rho_s[k-1] & & 1 + \sigma_s^2 \end{bmatrix}$$

When the probability distribution is found for all ISI lengths, its coefficient of variation is calculated as $CV^2 = \frac{\mathrm{var}(P)}{\langle P \rangle^2}$

Count correlations of de novo spike trains

Spike count correlation coefficient by definition is

$$CC = \frac{\mathrm{cov}\left(\sum_{n=1}^{N} r^p[n], \sum_{m=1}^{N} r^q[m]\right)}{\sqrt{\mathrm{var}\left(\sum_{n=1}^{N} r^p[n]\right) \mathrm{var}\left(\sum_{m=1}^{N} r^q[m]\right)}}$$

$$= \frac{\left\langle \left(\sum_{n=1}^{N} r^p[n]\right)\left(\sum_{m=1}^{N} r^q[m]\right)\right\rangle - \left\langle \sum_{n=1}^{N} r^p[n]\right\rangle \left\langle \sum_{m=1}^{N} r^q[m]\right\rangle}{\sqrt{\mathrm{var}\left(\sum_{n=1}^{N} r^p[n]\right)\mathrm{var}\left(\sum_{m=1}^{N} r^q[m]\right)}}$$

where similarly to the analogous formula for Fano factor

$$\left\langle \sum_{n=1}^{N} r^p[n] \sum_{m=1}^{N} r^q[m] \right\rangle = \sum_{m=1}^{N}\sum_{n=1}^{N} \Phi_2\left(\begin{matrix} -\theta^p \\ -\theta^q \end{matrix}, \Sigma_s[m-n] + \Sigma_z[m-n] \right)$$

and

$$\mathrm{var}\left(\sum_{n=1}^{N} r^p[n]\right) = N\Phi\left(-\theta^p, \sigma_{s^p}^2 + 1\right) + \sum_{n=1}^{N}\sum_{m=1}^{N} \Phi_2\left(\begin{matrix} -\theta^p \\ -\theta^p \end{matrix}, \begin{bmatrix} \sigma_{s^p}^2 + 1 & \rho_z^{pp}[m-n] \\ \rho_z^{pp}[m-n] & \sigma_{s^p}^2 + 1 \end{bmatrix} \right) - \left(N\Phi\left(-\theta^p, \sigma_{s^p}^2 + 1\right)\right)^2$$

where, in turn, assuming symmetry of correlations

$$\Sigma_s[m-n] = \begin{bmatrix} \sigma_{s^p}^2 & \sigma_{s^p}\sigma_{s^q}\rho_s^{pq}[m-n] \\ \sigma_{s^p}\sigma_{s^q}\rho_s^{pq}[m-n] & \sigma_{s^q}^2 \end{bmatrix}$$

$$\Sigma_s[m-n] = \begin{bmatrix} 1 & \rho_z^{pq}[m-n] \\ \rho_z^{pq}[m-n] & 1 \end{bmatrix}$$

This formula can be used to analyze the dependencies of count correlation on single cell and pairwise parameters. For example, because the variances of spike counts in the denominator of the expression for count correlations depend only on autocorrelations, but not on cross correlations, one can see that an increase in autocorrelations (which leads to an increase in Fano factor) decreases count correlations when crosscorrelations and other parameters are fixed.

Independent manipulation of CV^2 and FF

In the ''Modelling experimental spike trains'' section, we showed how, by using the version of the dichotomized Gaussian model with temporal correlations, one can match and manipulate different parameters of variability and covariability in experimental responses. In those examples, the different measures of variability and covariability were considered independently of each other, though all may be affected by changes in the auto- and cross correlation functions of the spike trains. However, independent manipulation of different types of variability is also possible if the correlation functions are parameterized by multiple parameters.

For example, both Fano factor and CV^2 are influenced by autocorrelations, but do not necessarily determine each other. For example, in the case of a homogeneous binary process (the case of a constant s in our model), the relationship between Fano factor and CV^2 of the ISI distribution is expressed as (Cox and Lewis 1966).

$$FF = CV^2\left(1 + \sum_{k=1}^{\infty} \rho_{serial}(k)\right)$$

Serial correlations $\rho_{serial}(k)$ are, in turn, functions of autocorrelations of z and their sum will depend on the shape of the autocorrelation functions. Hence, in this simple case one can potentially manipulate CV^2 and Fano factor independently of one another by changing the sum of the serial correlation coefficients by changing the autocorrelation functions.

To provide a more complex example of the independent manipulation of Fano factor and CV^2 of the ISI distribution in our model, we parameterized autocorrelation functions with a family of functions with two free parameters (α, β) that model both refractory spiking and burstiness:

$$\rho_z[k] = \begin{cases} 1, & k = 0 \\ e^{-\alpha k} - 2e^{-\beta k} & k \geq 1 \end{cases}$$

The sum of exponents allows for different positive overshoots after a refractory period, which in turn will make it possible to have several different values of Fano factor for a given value of CV^2.

First, we investigated how *FF* and CV^2 change with the changing parameters of the autocorrelation functions, and then investigated how *FF* changes along the lines on the (α, β) plane where the CV^2 stays constant. This analysis demonstrates the degree to which Fano factor and CV^2 can be manipulated independently. For this purpose, we created two examples – one in which s is a Gaussian process as in the *de novo* framework described above, and another one in which s is an arbitrary deterministic signal in the form of a sine wave (see figure legend for details).

Figure 5A shows the values of CV^2 for a range of parameters of the described family of functions in the case of sine wave s. For certain combinations of parameters (α, β), the autocorrelation functions result in covariance matrices of z that are not positive-definite, and thus the process is not realizable. This region of parameter space is shown in white. For all the other possible combinations of parameter values within the range selected for this illustration (α between 0 and 2, and beta between 0 and 5), different values of CV^2 are shown in different colors from blue for the lowest values to red for the highest. We chose three values of interest: $CV^2 = 5.5$, $CV^2 = 5.7$, $CV^2 = 5.9$ and plotted the lines along which the values of CV^2 were equal to these values (shown in red). At the ends of the lines of equality we plotted the autocorrelations of z that correspond to the combination of parameters at the given end. From these plots, one can see that the same values of CV^2 can be achieved for different autocorrelation functions. Next, as shown in Figure 5B, we calculated the Fano factors along each iso-CV^2 curve. The insets show autocorrelation functions for the corresponding set of parameters at both ends of the curves (marked with black circles). Figure 5B shows that Fano factor changes considerably along the iso-CV^2 curves and, thus, there is a room for independent manipulation of CV^2 and Fano factor. However, when we chose s to be a Gaussian random process rather than a sine wave and performed the same analysis as above, the results were somewhat different. As shown in Figure 5C, even though the autocorrelation functions change along the lines of equality for CV^2, the range of Fano factors is less that in the case of sinusoidal s. Thus, in this case, there is less room for independent manipulation of CV^2 and Fano factor.

The results in Figure 5 suggest a strong influence of the signal itself on the statistics of the resulting spike trains. To investigate this issue in more detail, we chose one particular correlation function from the family of functions described

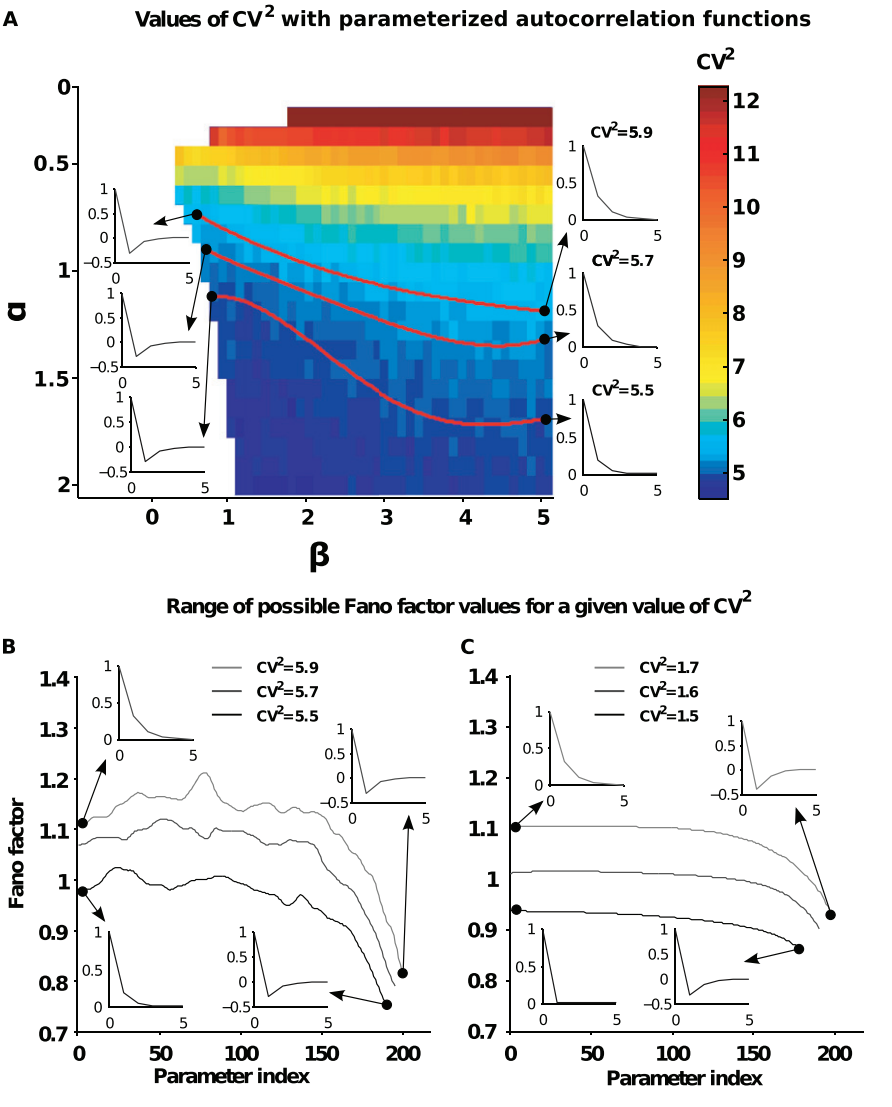

Figure 5. Map of values of CV^2 in space of parameters of autocorrelation function of s. The family of functions that we model autocorrelation functions with is described in the "Independent manipulation of CV^2 and FF" section. The parameters α and β were varied between 0 and 2, and 0 and 5 correspondingly. Colorbar to the right of the map shows the actual values of CV^2 for the corresponding color. Red lines on the map show lines of equality for CV^2 of 5.5, 5.7, and 5.9. Sample autocorrelation functions are plotted next to the ends of isolines as insets (the corresponding ends are marked with black dots and arrows). The map is created by sampling from a model in which s is a sine wave with frequency of 1.6 Hz, amplitude of 1, and zero mean. The threshold was chosen such that the average spiking rate was 60 spikes per second. The simulations were 1 second long, binned in 1000 time bins each and had 1000 trials for every autocorrelation function. B. Range of changes in Fano factor along the lines of equality of CV^2. Using the map of CV^2 values in two-parameter space (A), we calculated Fano factor for all the pairs of parameters (in the given range) where CV^2 is constant and equal to 5.5, 5.7, and 5.9. The horizontal axis shows the index of the pair of parameters (that increases as the values of parameters α and β decrease), and the vertical axis shows the value of Fano factor for this combination of parameters. Insets show plots of the autocorrelation functions on the corresponding ends of

continued

above (with $\alpha = 0.3$ and $\beta = 1.5$), and varied the frequency of the sinusoidal signal and its amplitude relative to the intrinsic noise.

In the stimulus driven case (high signal amplitude), the CV^2 values changed substantially with changing frequency. As expected, in the noise driven case (with low signal amplitude), changes in frequency had no significant effect on the ISI distributions and hence the CV^2 values. The figure shows that similar values of CV^2 can be achieved through different combinations of signal and noise parameters, and through different ISI distributions. We did the same analysis for several other, qualitatively different functions from the same family, and found that the behavior of the curves is similar for all of them.

These examples demonstrate that, although our framework can be used to vary different measures of variability and covariability independently, the extent to which this is possible can depend strongly on the stimulus.

Limitations of the model

We have shown how our model can be applied to spike trains with a range of different statistical properties. However the dichotomized Gaussian framework has limitations as well, as have been noted before (Macke et al. 2009; Gutnisky and Josić 2010), most of which stem from the fact that the covariance matrices of Gaussian processes must be positive-definite. This constraint imposes limitations on the allowed auto- and crosscorrelation functions that can be used in our model.

In particular, one strong limitation of the model is that only weak negative correlations can be reproduced (Macke et al. 2009; Gutnisky and Josić 2010). The ability of our model to capture weak negative correlations has been illustrated in the ''Variability of single cells on short time scales: ISI distributions'' section, where we reproduced the refractory period of experimental spike trains, and then increased it, such that the spiking became even more regular. However, as shown in Figure 7A, the model is incapable of generating spike trains with strong negative correlations.

The red line shows the values of the autocorrelations of z that would be required to match the autocorrelations in a set of spike trains with a strong refractory period recorded from the IC. The covariance matrix corresponding to these values is not positive definite, and thus the process is not realizable. We scaled the values and weakened the negative autocorrelations until we obtained a realizable process, resulting in the values shown in black.

figure continued
curves (marked with dots and arrows). C. Range of changes in Fano factor along the lines of equality of CV^2. We created a map analogous to the one shown in A (not shown here) but with the s component in the generative process being a Gaussian process without temporal correlations and with variance of 0.4. We chose to consider the range of changes in Fano factor for the isolines with CV^2 equal to 1.5, 1.6, and 1.7. The plot shows three corresponding curves with increasing values CV^2 of from bottom to top. As in B, the horizontal axis shows index of the pair of parameters (that increases as the values of parameters α and β decrease), and the vertical axis shows the value of Fano factor for this combination of parameters. Insets show plots of the autocorrelation functions on the corresponding ends of curves (marked with dots and arrows).

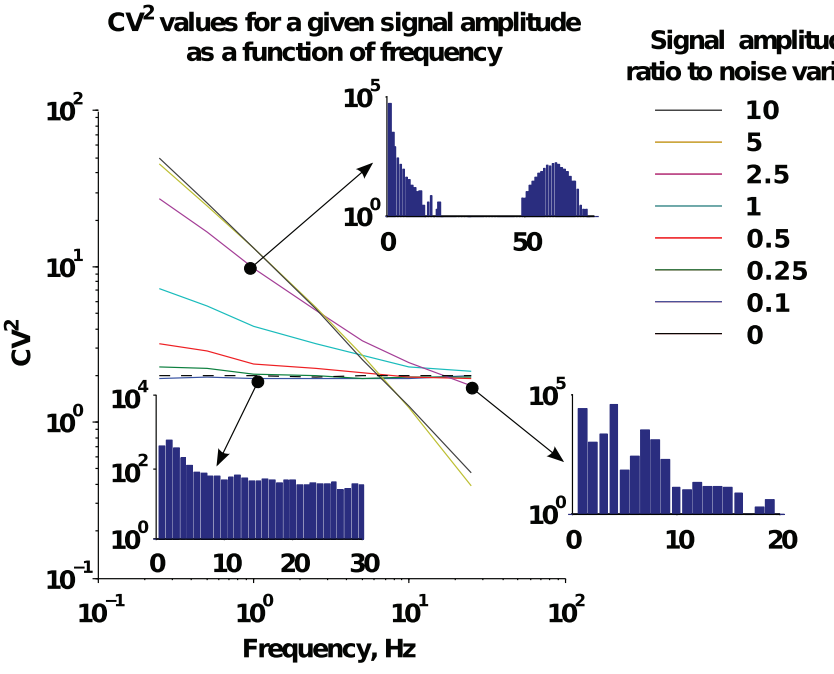

Figure 6. CV^2 of the ISI distribution as a function of amplitude and frequency of the sinusoidal signal. We varied the amplitude of signal from 0.1 to 10 with the amplitude of noise always being 1. The frequency was varied between 0.16 and 40 Hz (note that the frequency axis has logarithmic scale). Simulations were done in 200 trials for each point, were 1 second long and binned in 1000 time bins. All the curves are plotted for the same autocorrelation function chosen from the family described in the "Independent manipulation of CV^2 and FF" section with $\alpha = 0.3$ and $\beta = 1.5$, which corresponds to a positive non-monotonically decreasing function. Dashed line shows the case when signal is completely absent. Histograms in the smaller insets show the ISI distributions for the marked points on the curves. The horizontal axis shows the length of ISIs in ms, and the vertical axis shows the number of occurrences of an ISI of a given length. With the wide range of relative amplitudes of signal one can see the behavior of the model in signal driven (high amplitude) and noise driven (low amplitude) cases. In the signal driven cases ISI histograms are defined by the structure of the signal (see the histograms on top and on the right having the periodic features of the corresponding signals), and in the noise driven cases, changes in signal frequency do not affect the ISI distribution in any significant way. The figure also illustrates that similar CV^2 values can be achieved in both signal and noise driven regimes and have qualitatively different underlying ISI distributions (compare the two lower histograms). Note that curves are plotted in logarithmic axes.

When a process is close to unrealizable, the strongest realizable correlations, and the behavior of the process that is generated, depend on the maximum lag at which the correlations are specified. In the example in Figure 7A, we only specified the autocorrelation function of z at lags 1 to 4. However, when we then used our model to generate a set of spike trains, the resulting spike trains contained significant positive autocorrelations at lag 5, as shown in black in Figure 7B. If one deliberately sets a zero correlation coefficient for z at lag 5, the positive autocorrelations in the spike trains are simply delayed to lag 6. This procedure, of explicitly setting zero correlation coefficients at successively larger lags, ultimately leads to a non-positive definite covariance matrix for z, and thus an unrealizable process (note that this

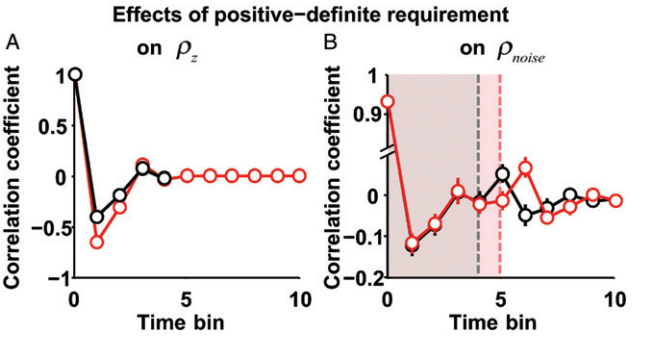

Figure 7. Effects of positive definite requirement on the covariance matrix of z. A. Example of the autocorrelation function of z calculated from the experimental data (red), and the closest realizable autocorrelation function (black). B. The attempt to reproduce strong negative correlations also leads to an artifact in the resulting spike trains. We simulated spike trains with correlations in time extending to the time bin 4 (no significant correlations beyond that limit in the original data), the simulated dataset had an artifact of significant positive correlations in time bin 5. When zero-padded (we deliberately added zero correlations to the time bin 5 in the correlation function of z), the artifact peak shifted to the next time bin. Further zero-padding resulted in a process that was unrealizable.

artifact is present not only in the spike train correlations, but also in the z process itself). This example illustrates the importance of choosing the range of autocorrelations carefully, and verifying that the corresponding model is realizable and can generate spike trains with the desired statistics.

Because of the limitations on the negative autocorrelation functions, values of Fano factor cannot be arbitrarily small. Similarly, ISI distributions that require a strong refractory period may not be realizable.

Discussion

The variability of single neurons and the covariability of neuronal populations can be measured on multiple time scales from synchrony in precise spike timing to correlations in spike count over a period of seconds. In previous work, we demonstrated the ability of a dichotomized Gaussian framework to reproduce the instantaneous variability in single neurons, and the instantaneous signal and noise correlations (i.e. synchrony) in neuronal populations (Lyamzin et al. 2010). In this study, we have shown how the dichotomized Gaussian model can capture variability and covariability on multiple time scales, and demonstrated its success in capturing the Fano factor, ISI distributions, and count correlations in experimental spike trains.

Our main motivation for developing the model was to enable the systematic study of different response properties of neuronal populations that cannot be easily decoupled experimentally. For example, to determine the time scales at which variability is important for coding a particular stimulus parameter, it is helpful to be able to manipulate the variability on different time scales independently. While this manipulation may be difficult to achieve experimentally (any change in the spike train autocorrelation function is likely to affect variability on multiple timescales), it may be achievable within our model framework with appropriate

parameterization. For example, as shown in the ''Independent manipulation of CV^2 and FF'' section, Fano factor and CV^2 of the interspike interval distribution can be manipulated independently under certain conditions.

Our model can also be used to systematically investigate the dependencies between different properties of spike trains. For example, our model framework captures the dependency of correlations on spike rate demonstrated in (De La Rocha et al. 2007) and analyzed in-depth in (Macke et al. 2011). Because our model captures the full second order structure of population spike trains, it should prove to be a useful tool for studying a wide range of such dependencies, as well as for determining how the value of a given response property constrains the possible range of possible values of others. For example, if one assumes that only second order correlations and stimulus affect the values of Fano factor and CV^2, our model provides a way to investigate the dependencies between them. Another example would be the inverse dependency of count correlations on the temporal autocorrelations of individual neurons, when pairwise correlations remain fixed, as noted in the ''Count correlations of *de novo* spike trains'' section.

We have also shown that the framework has significant limitations, the most important of which is the inability to generate or model spike trains with strong negative correlations. This limitation arises from the requirement that the covariance matrix of the multivariate Gaussian process z is positive definite. Note that this limitation is inherent to the model framework, and is independent of the specific method used to generate the Gaussian process when simulating spike trains (Gutnisky and Josić 2010). Because of this limitation, the model is better suited to modelling spike trains from cortical areas where correlations are typically positive (Bair et al. 2001; Smith and Kohn 2008) than subcortical areas where strong negative correlations due to refractory effects may be prominent.

Another limitation of our model is that it is only designed to capture the first and second order statistical properties of spike trains and may not accurately reflect higher order properties, such as the dependencies between successive ISIs or correlations among groups of neurons that are not predictable from second order statistics. This limitation may be important for certain brain areas where higher order correlations carry significant information (Ohiorhenuan et al. 2010, Farkhooi et al. 2009,

Nesse et al. 2010). One should note that even though the dichotomized Gaussian does not allow for explicit control of higher-order correlations, it still produces them as a result of the thresholding process (Macke et al. 2011). Interestingly, the higher-order correlations produced by the Gaussian model correspond well to the higher-order correlations found in cortex (Yu et al. 2012). These results suggest that models based on the dichotomized Gaussian framework are potentially promising for research into the effects of higher-order correlations on coding, although further experimental study of this issue is needed.

Acknowledgements

The authors thank Jakob Macke and Maneesh Sahani for helpful discussions. This work was supported by the German Research Foundation (DFG) and the Wellcome Trust.

Declaration of interest: The authors report no conflicts of interest. The authors alone are responsible for the content and writing of the paper.

References

Abbott LF, Dayan P. 1999. The effect of correlated variability on the accuracy of a population code. Neural Computation 11(1):91–101.

Averbeck BB, Latham PE, Pouget A. 2006. Neural correlations, population coding and computation. Nature Reviews Neuroscience 7(5):358–66.

Bair W, Zohary E, Newsome WT. 2001. Correlated firing in macaque visual area MT: Time scales and relationship to behavior. The Journal of Neuroscience: The Official Journal of the Society for Neuroscience 21(5):1676–1697.

Berry MJ, Warland DK, Meister M. 1997. The structure and precision of retinal spike trains. Proceedings of the National Academy of Sciences of the United States of America 94(10):5411–5416.

Buracas GT, Zador A, DeWeese M, Albright TD. 1998. Efficient discrimination of temporal patterns by motion-sensitive neurons in primate visual cortex. Neuron 20(5):959–969.

Cox DR, Lewis PAW. 1966. The statistical analysis of series of events London: Methuen.

Dan Y, Alonso JM, Usrey MW, Reid CR. 1998. Coding of visual information by precisely correlated spikes in the lateral geniculate nucleus. Nature Neuroscience 1(6):501–507.

Farkhooi F, Strube-Bloss MF, Nawrot MP. 2009. Serial correlation in neural spike trains: experimental evidence, stochastic modeling, and single neuron variability. Physical Review E 79(2 Pt 1):021905.

Gershon ED, Wiener MC, Latham PE, Richmond BJ. 1998. Coding strategies in monkey V1 and inferior temporal cortices. Journal of Neurophysiology 79(3):1135–1144.

Gur M, Beylin A, Snodderly DM. 1997. Response variability of neurons in primary visual cortex (V1) of alert monkeys. The Journal of Neuroscience: The Official Journal of the Society for Neuroscience 17(8):2914–2920.

Gutnisky DA, Josić K. 2010. Generation of spatiotemporally correlated spike trains and local field potentials using a multivariate autoregressive process. Journal of Neurophysiology 103(5):2912–2930.

Hartveit E, Heggelund P. 1994. Response variability of single cells in the dorsal lateral geniculate nucleus of the cat. Comparison with retinal input and effect of brain stem stimulation. Journal of Neurophysiology 72(3):1278–1289.

Kara P, Reinagel P, Reid RC. 2000. Low response variability in simultaneously recorded retinal, thalamic, and cortical neurons. Neuron 27(3):635–646.

Krumin M, Shoham S. 2009. Generation of spike trains with controlled auto-and cross-correlation functions. Neural Computation 21:1642–1664.

De La Rocha J, Doiron B, Shea-Brown E, Josić K, Reyes A. 2007. Correlation between neural spike trains increases with firing rate. Nature 448:802–806.

Latham PE, Nirenberg S. 2005. Synergy, redundancy, and independence in population codes, revisited. The Journal of Neuroscience: The Official Journal of the Society for Neuroscience 25(21):5195–5206.

Lyamzin DR, Macke JH, Lesica NA. 2010. Modeling population spike trains with specified time-varying spike rates, trial-to-trial variability, and pairwise signal and noise correlations. Frontiers in Computational Neuroscience 4:144.

MacKay D. 2003. Information theory, inference, and learning algorithms Cambridge, UK; New York: Cambridge University Press.

Macke JH, Opper M, Bethge M. 2011. Common input explains higher-order correlations and entropy in a simple model of neural population activity. Physical Review Letters 106(20):208102.

Macke JH, Berens P, Ecker AS, Tolias AS, Bethge M. 2009. Generating spike trains with specified correlation coefficients. Neural Computation 21(2):397–423.

Mainen ZF, Sejnowski TJ. 1995. Reliability of spike timing in neocortical neurons. Science 268(5216):1503–1506.

Manwani A, Steinmetz PN, Koch C. 2002. The impact of spike timing variability on the signal-encoding performance of neural spiking models. Neural Computation 14(2):347–367.

Nawrot MP. 2010. Analysis and Interpretation of Interval and Count Variability in Neural Spike Trains. In: Grün S, Rotter S, editors. Analysis of Parallel Spike Trains. Boston, MA: Springer US. pp 37–58.

Nawrot MP, Boucsein C, Molina VR, Riehle A, Aertsen A, Rotter S. 2008. Measurement of variability dynamics in cortical spike trains. Journal of Neuroscience Methods 169(2):374–390.
Nesse WH, Maler L, Longtin A. 2010. Biophysical information representation in temporally correlated spike trains. Proceedings of the National Academy of Sciences of the United States of America 107(51):21973–21978.
Ohiorhenuan IE, Mechler F, Purpura KP, Schmid AM, Victor JD. 2010. Sparse coding and high-order correlations in fine-scale cortical networks. Nature 466:617–621.
Oram MW, Wiener MC, Lestienne R, Richmond BJ. 1999. Stochastic nature of precisely timed spike patterns in visual system neuronal responses. Journal of Neurophysiology 81(6):3021–3033.
Puchalla JL, Schneidman E, Harris RA, Berry MJ 2nd. 2005. Redundancy in the population code of the retina. Neuron 46(3):493–504.
Ratnam R, Nelson ME. 2000. Nonrenewal statistics of electrosensory afferent spike trains: Implications for the detection of weak sensory signals. The Journal of Neuroscience: The Official Journal of the Society for Neuroscience 20(17):6672–6683.
Romo R, Hernandez A, Zainos A, Salinas E. 2003. Correlated neuronal discharges that increase coding efficiency during perceptual discrimination. Neuron 38(4):649–657.
Schneidman E, Bialek W, Berry MJ 2nd. 2003. Synergy, redundancy, and independence in population codes. The Journal of Neuroscience: The Official Journal of the Society for Neuroscience 23(37):11539–11553.
Schneidman E, Freedman B, Segev I. 1998. Ion channel stochasticity may be critical in determining the reliability and precision of spike timing. Neural Computation 10(7):1679–1703.
Sestokas AK, Lehmkuhle S. 1988. Response variability of X- and Y-cells in the dorsal lateral geniculate nucleus of the cat. Journal of Neurophysiology 59(2):317–325.
Shadlen MN, Newsome WT. 1998. The variable discharge of cortical neurons: Implications for connectivity, computation, and information coding. The Journal of Neuroscience: The Official Journal of the Society for Neuroscience 18(10):3870–3896.
Shimokawa T, Koyama S, Shinomoto S. 2010. A characterization of the time-rescaled gamma process as a model for spike trains. Journal of Computational Neuroscience 29(1-2):183–191.
Smith MA, Kohn A. 2008. Spatial and temporal scales of neuronal correlation in primary visual cortex. Journal of Neuroscience 28:12591.
Softky WR, Koch C. 1993. The highly irregular firing of cortical cells is inconsistent with temporal integration of random EPSPs. The Journal of Neuroscience: The Official Journal of the Society for Neuroscience 13(1):334–350.
Tchumatchenko T, Giesel T, Volgushev M, Wolf F. 2010. Signatures of synchrony in pairwise count correlations. Frontiers in Computational Neuroscience 4:1.
Tolhurst DJ, Movshon JA, Dean AF. 1983. The statistical reliability of signals in single neurons in cat and monkey visual cortex. Vision Research 23(8):775–785.
Vaadia E, Haalman I, Abeles M, Bergman H, Prut Y, Slovin H, Aertsen A. 1995. Dynamics of neuronal interactions in monkey cortex in relation to behavioural events. Nature 373(6514):515–518.
Yu S, Yang H, Nakahara H, Santos GS, Nicolić D, Plenz D. 2012. Higher-order interactions characterized in cortical activity. The Journal of Neuroscience: The Official Journal of the Society for Neuroscience 31(48):17514–26.
Zohary E, Shadlen MN, Newsome WT. 1994. Correlated neuronal discharge rate and its implications for psychophysical performance. Nature 370(6485):140–143.

Appendix A

By definition, Fano factor is the ratio of spike count variance and mean spike count across the trials.

$$FF = \frac{\mathrm{var}\left(\sum_{n=1}^{N} r[n]\right)}{\left\langle \sum_{n=1}^{N} r[n] \right\rangle} = \frac{\left\langle \left(\sum_{n=1}^{N} r[n]\right)^2 \right\rangle - \left\langle \sum_{n=1}^{N} r[n] \right\rangle^2}{\left\langle \sum_{n=1}^{N} r[n] \right\rangle}$$

(because Fano factor is a single cell quantity, cell indices are omitted for simplicity). We expand the square of the spike count to deal with the expected values of the elements of this expansion.

$$\left(\sum_{n=1}^{N} r[n]\right)^2 = r[1]r[1] + r[1]r[2] + \cdots + r[n]r[m] + \cdots + r[N]r[N]$$

Since r is a binary vector, $r[n]r[n] = r[n]$ and thus $\langle r[n]r[n]\rangle = \Phi(s[n], 1)$.

We define correlation matrix

$$\Sigma_z[k] = \begin{bmatrix} 1 & \rho_z[k] \\ \rho_z[k] & 1 \end{bmatrix}$$

then rewrite the expression for the square of the spike count as follows:

$$\left\langle \left(\sum_{n=1}^{N} r[n]\right)^2 \right\rangle = \left\langle \sum_{n=1}^{N} r[n]r[n] + 2\sum_{m=n+1}^{N}\sum_{n=1}^{N} r[n]r[m] \right\rangle$$
$$= \sum_{n=1}^{N} \Phi(s[n], 1) + 2\sum_{m=n+1}^{N}\sum_{n=1}^{N} \Phi_2\left(\begin{matrix} s[n] \\ s[m] \end{matrix}, \Sigma_z[m-n]\right)$$

and the full expression for Fano factor is

$$FF = \frac{\sum_{n=1}^{N} \Phi(s[n], 1) + 2\sum_{m=n+1}^{N}\sum_{n=1}^{N} \Phi_2\left(\begin{matrix} s[n] \\ s[m] \end{matrix}, \Sigma_z[m-n]\right) - \left(\sum_{n=1}^{N} \Phi(s[n], 1)\right)^2}{\sum_{n=1}^{N} \Phi(s[n], 1)}.$$

Appendix B

Fano factor by definition is

$$FF = \frac{\mathrm{var}\left(\sum_{n=1}^{N} r[n]\right)}{\left\langle \sum_{n=1}^{N} r[n] \right\rangle} = \frac{\left\langle \left(\sum_{n=1}^{N} r[n]\right)^2 \right\rangle - \left\langle \sum_{n=1}^{N} r[n] \right\rangle^2}{\left\langle \sum_{n=1}^{N} r[n] \right\rangle}$$

(because Fano factor is a single cell quantity, cell indices are omitted for simplicity). Expanding the first term in the numerator we get

$$\left(\sum_{n=1}^{N} r[n]\right)^2 = r[1]r[1] + \cdots + r[m]r[n] + \cdots + r[N]r[N]$$

Where each $r[n]r[n]$ term equals $r[n]$ because r is a binary vector.

$$\langle r[n]r[n]\rangle = \langle r[n]\rangle = \langle s[n] + z[n] > \theta\rangle = \Phi(-\theta, \sigma_s^2 + 1)$$

For all the other products $r[n]r[m]$ where $n \neq m$

$$\langle r[n]r[m]\rangle = \Phi_2\left(\begin{matrix}-\theta\\-\theta\end{matrix}, \Sigma_{s+z}[m-n]\right)$$

Where Φ_2 is a two-dimensional Gaussian cumulative distribution function, and we define Σ_{s+z} as

$$\Sigma_{s+z}[m-n] = \begin{bmatrix} \sigma_s^2 + 1 & \rho_z[m-n] + \sigma_s^2\rho_z[m-n] \\ \rho_z[m-n] + \sigma_s^2\rho_z[m-n] & \sigma_s^2 + 1 \end{bmatrix}$$

Hence the final formula for Fano factor is (assuming symmetry of correlations)

$$FF = \frac{\sum_{n=1}^{N}\Phi\left(-\theta, \sigma_s^2+1\right) + \sum_{n\neq m}^{N}\Phi_2\left(\begin{matrix}-\theta\\-\theta\end{matrix}, \Sigma_{s+z}[m-n]\right) - \left(\sum_{n=1}^{N}\Phi\left(-\theta, \sigma_s^2+1\right)\right)^2}{\left(\sum_{n=1}^{N}\Phi\left(-\theta, \sigma_s^2+1\right)\right)}$$